8276 *Inorg. Chem.* **2009**, *48*, 8276–8285
DOI: 10.1021/ic900971h

Inorganic Chemistry
Article

Lanthanide (Eu^{3+}, Tb^{3+})/β-Diketone Modified Mesoporous SBA-15/Organic Polymer Hybrids: Chemically Bonded Construction, Physical Characterization, and Photophysical Properties

Ya-Juan Li and Bing Yan*

Department of Chemistry, Tongji University, Siping Road 1239, Shanghai 200092, China

Received May 18, 2009

Novel organic−inorganic mesoporous luminescent polymeric hybrid materials containing lanthanide (Eu^{3+}, Tb^{3+}) complexes covalently bonded to mesoporous silica SBA-15 have been successfully prepared by co-condensation of the modified 2-thenoyltrifluoroacetone (TTA−Si) and tetraethoxysilane (TEOS) in the presence of Pluronic P123 surfactant as a template. 2Z-Thenoyltrifluoroacetone (TTA) was grafted onto the coupling agent 3-(triethoxysilyl)-propyl isocyanate (TEPIC) and used as the first precursor, and the other precursor PMMA was synthesized through the addition polymerization reaction of the monomer methyl methacrylate. Then these precursors coordinated to rare earth ions, and the final mesoporous polymeric hybrid materials Ln(TTA-SBA-15)$_3$PMMA (Ln = Eu, Tb) were obtained after hydrolysis and copolycondensation with the tetraethoxysilane (TEOS) via a sol−gel process. In addition, for comparison, SBA-15 covalently bonded with the binary Ln^{3+} complexes with TTA ligand were also synthesized, denoted as Ln(TTA-SBA-15)$_3$ (Ln = Eu, Tb). All of these hybrid materials have high surface area, uniformity in the mesostructure, and good crystallinity. The detailed luminescence studies on all the materials showed that the ternary rare-earth mesoporous polymeric hybrid materials present stronger luminescent intensities, longer lifetimes, and higher luminescent quantum efficiencies than the binary rare-earth mesoporous hybrid materials, indicating that the introduction of the organic polymer chain is a benefit for the luminescence properties of the overall hybrid system.

1. Introduction

Inorganic−organic hybrid materials have attracted considerable attention because of their extraordinary properties in many fields of applications as they combine the respective characteristics of organic and inorganic parts.[1−4] Among all the synthetic methods, the sol−gel approach which is based on hydrolysis/polycondensation reactions of metal alkoxides is considered as an excellent approach for the preparation of such hybrid compounds.[5,6] The potential advantages of the sol−gel route with respect to other classical synthetic procedures include relatively low-temperature processing, higher purity, improvement of the thermal and dimensional stability of the resulting compounds.[7−11] In addition, this mild synthetic method allows the composites to exhibit high versatility, offering a wide range of chances for preparation of tailor-made materials in terms of their unique features. In particular, the microstructure, the external shape or the degree of combination between the two phases can be controlled by changing the sol−gel reaction conditions.[12,13] It is well-known that lanthanide complexes have characteristic luminescence properties and show sharp, intense emission bands upon ultraviolet light irradiation because of the effective intramolecular energy transfer from the coordinated ligands to the luminescent central lanthanide ions.[14−16] In the past few decades, metal complexes doped into inorganic matrixes, especially recently, hybrids of lanthanide organic complexes introduced in silica gel have already been found to display characteristic emission intensities compared with

*To whom correspondence should be addressed. E-mail: byan@tongji.edu.cn. Fax: +86-21-65982287. Phone: +86-21-65984663.

(1) Wen, J.; Wilkes, G. L. *Chem. Mater.* **1996**, *8*, 1667.
(2) Sanchez, C.; Babonneau, F. *Matériaux Hybrides*; Observatoire Francais des Techniques Avancées, Masson: Paris, 1996.
(3) Franville, A. C.; Zambon, D.; Mahiou, R. *Chem. Mater.* **2000**, *12*, 428.
(4) Molina, C.; Dahmouche, K.; Santilli, C. V.; Craievich, A. F.; Ribeiro, S. J. L. *Chem. Mater.* **2001**, *13*, 2818.
(5) Stein, A.; Melde, B. J.; Schroden, R. C. *Adv. Mater.* **2000**, *12*, 1403.
(6) Sanchez, C.; Soler-Illia, G. J. de A. A.; Ribot, F.; Lalot, T.; Mayer, C. R.; Cabuil, V. *Chem. Mater.* **2001**, *13*, 3061.
(7) Goncüalves, M. C.; Bermudez, V. Z.; Ferreira, R. A.; Carlos, L. D.; Ostrovskii, D.; Rocha, J. *Chem. Mater.* **2004**, *16*, 2530.
(8) Casalboni, M.; Senesi, R.; Prospositio, P. *Appl. Phys. Lett.* **1997**, *30*, 2969.
(9) Lebeau, B.; Fowler, C. E.; Hall, S. R. *J. Mater. Chem.* **1999**, *9*, 2279.
(10) Innocenzi, P.; Kozuka, H.; Yoko, T. J. *J. Phys. Chem. B.* **1997**, *101*, 2285.
(11) Mstsui, K.; Momose, F. *Chem. Mater.* **1997**, *9*, 2588.
(12) Judeinstein, P.; Sanchez, C. *J. Mater. Chem.* **1996**, *6*, 511.
(13) Schubert, U. *J. Chem. Soc., Dalton Trans.* **1996**, *16*, 3343.
(14) Sabbatini, N.; Guardingli, M.; Lehn, J. M. *Coord. Chem. Rev.* **1993**, *123*, 201.
(15) Reisfeld, R. *Struct. Bonding* (*Berlin*) **2004**, *106*, 209.
(16) DeSa′, G. F.; Malta, O. L.; Donega′, C. D.; Simas, A. M.; Longo, R. L.; Santa-Cruz, P. A.; da Silva, E. F. *Coord. Chem. Rev.* **2000**, *196*, 165.

 Published on Web 07/31/2009

lanthanide ions doped into inorganic hosts. Organic components are regarded to be efficient sensitizers for the luminescence of lanthanide ions, namely, the antenna effect.[17,18] They also reduce both the concentration and the OH quenching, which have shown to be very important in siloxane matrixes.[19−21] Therefore, extensive work has been carried out on entrapping of rare-earth complexes with β-diketones, aromatic carboxylic acids, and heterocyclic ligands into sol−gel derived host structures.[22,23] Typically, these materials were obtained by doping silica gels with organometallic complexes and were called Class I hybrid materials. However, since there are only weak interactions (typically hydrogen bonds or van der Waals forces) between organic and inorganic parts, it is difficult to prevent clustering of emitting centers, and the dispersion of both components is inhomogeneous. Also, there exists a concentration limit for doping the organic species, since the resulting hybrids become brittle when the gel solution contains large amounts of complexes. In addition, leaching of the complexes was also observed in these Class I hybrid materials.[24] Therefore, attention has been paid to grafting the ligands covalently to the silica backbone via Si−C bonds to obtain Class II hybrid materials. The as-derived molecular-based luminescent materials were monophasic even at a high concentration of organic chelates, and the reinforcement of thermal and mechanical resistances has been clearly established.[3,25−28] Our research group is dedicated to the design of the rare-earth hybrid materials with inorganic networks.[29−37] Compared to chemically bonded rare-earth hybrids with Si−O polymeric networks, fewer reports on molecular hybrid materials fabricated with rare-earth/organic polymers have been published,[38−43] although these hybrid materials can exhibit the infinite chain polymeric structure similar to an organic polymer matrix and strong luminescence with high stability.

In the past few years, the mesoporous molecular sieves (MMSs) used as a support for lanthanide complexes have started to attract much attention since they offer many novel and unique properties, such as the rigidity, photostability, and well-defined hydrophilic/hydrophobic phase separation allowing for more sophisticated tuning of the lanthanide complex microenvironment.[44,45] As a host material for lanthanide complexes, SBA-15 appears to be more attractive than other mesoporous silicas because of its much larger uniform pore size (up to 30 nm), thicker silica wall, and better stability.[46,47] For example, the larger pores make it an attractive host for the insertion of large amounts of bulky molecules with functional properties, and better stability makes it very suitable for immobilization of functional molecules. Therefore, many research efforts, which have focused on preparing the organic/inorganic hybrids through functionalization of the exterior and/or interior surfaces, have promoted the utilization of mesoporous SBA-15 in many areas. It is shown that promising visible-luminescent properties can be obtained by linking the ternary lanthanide complexes to the mesoporous materials.[48,49]

In this article, we put forward a synthetic approach to assemble ternary hybrid materials containing mesoporous silicon and organic polymeric chains. We have synthesized 2-thenoyltrifluoroacetone (TTA) functionalized SBA-15 mesoporous hybrid material (TTA -SBA-15) as a host framework using a similar method to that in ref 35. Subsequently, the addition polymerization reaction was performed so as to synthesize the polymer PMMA containing the polymeric chains (C−C) using the monomer methyl methacrylate as the raw materials. Then, after the coordination reaction between rare earth ions, precursor, and the polymers and the hydrolysis cross-linking reaction, we obtained the final mesoporous polymeric hybrids Ln(TTA-SBA-15)$_3$PMMA (Ln = Eu, Tb). To the best of our knowledge, our results provide the demonstration of the assembly of ternary ordered mesoporous hybrid materials fabricated with organic polymeric chains. In addition, for comparison, binary SBA-15 mesoporous hybrids were also synthesized, denoted as Ln(TTA-SBA-15)$_3$ (Ln = Eu, Tb). Full characterization and detailed studies of the luminescence properties of all synthesized materials were investigated and compared.

2. Experimental Section

2.1. Chemicals. Pluronic P123 ($EO_{20}PO_{70}EO_{20}$, Aldrich), tetraethoxysilane (TEOS, Aldrich) and 3-(triethoxysilyl)-propyl isocyanate (TEPIC, Lancaster). The solvent tetrahydrofuran (THF) was used after desiccation with anhydrous calcium chloride. Ln$(NO_3)_3$ (Ln = Eu, Tb) ethanol solution (EtOH) were prepared by dissolving their respective oxides (Eu_2O_3 and

(17) Serra, O. A.; Nassar, E. J.; Rosa, I. L. V. *J. Lumin.* **1997**, *72−74*, 263.
(18) Bredol, M.; Kynast, U.; Boldhaus, M.; Lau, C. *Ber. Bunsen-Ges. Phys. Chem.* **1998**, *102*, 1557.
(19) Viana, B.; Koslova, N.; Aschehoug, P.; Sanchez, C. *J. Mater. Chem.* **1995**, *5*, 719.
(20) Campostrini, R.; Ferrari, M.; Montagna, M.; Pilla, O. *J. Mater. Res.* **1992**, *7*, 745.
(21) Lochhead, M.; Bray, K. L. *Chem. Mater.* **1995**, *7*, 572.
(22) Yan, B.; Zhang, H. J.; Wang, S. B.; Ni, J. Z. *Mater. Chem. Phys.* **1997**, *51*, 92.
(23) Li, H. R.; Zhang, H. J.; Lin, J.; Wang, S. B.; Yang, K. Y. *J. Non-Cryst. Solids* **2000**, *278*, 218.
(24) Sanchez, C.; Ribot, F. *New J. Chem.* **1994**, *18*, 1007.
(25) Lenaerts, P.; Storms, A.; Mullens, J.; Dhaen, J.; Gorller-Walrand, C.; Binnemans, K.; Driesen, K. *Chem. Mater.* **2005**, *17*, 5194.
(26) Franville, C.; Zambon, D.; Mahiou, R.; Chou, S.; Troin, Y.; Coussiens, J. C. *J. Alloys Compd.* **1998**, *275−277*, 837.
(27) Dong, D.; Jiang, S.; Men, Y.; Ji, X.; Jiang, B. *Adv. Mater.* **2000**, *12*, 646.
(28) Li, H. R.; Lin, J.; Zhang, H. J.; Li, H. C.; Fu, L. S.; Meng, Q. G. *Chem. Commun.* **2001**, 1212.
(29) Wang, Q. M.; Yan, B. *Inorg. Chem. Commun.* **2004**, *7*, 1124.
(30) Zhao, L. M.; Yan, B. *Appl. Organomet. Chem.* **2005**, *19*, 1060.
(31) Yan, B.; Zhao, L. M. *Mater. Lett.* **2005**, *59*, 795.
(32) Wang, Q. M.; Yan, B. *J. Photochem. Photobiol, A: Chem.* **2006**, *177*, 1.
(33) Wang, Q. M.; Yan, B. *J. Photochem. Photobiol, A: Chem.* **2005**, *175*, 159.
(34) Yan, B.; Wang, F. F. *J. Organomet. Chem.* **2007**, *692*, 2395.
(35) Li, Y.; Yan, B.; Yang, H. *J. Phys. Chem. C.* **2008**, *112*, 3959.
(36) Liu, J. L.; Yan, B. *J. Phys. Chem. C.* **2008**, *112*, 14168.
(37) Liu, J. L.; Yan, B. *J. Phys. Chem. B.* **2008**, *112*, 10898.
(38) Iwamura, R.; Higashiyama, N.; Takemura, K.; Tsutsumi, S.; Kimura, K.; Adachi, G. *Chem. Lett.* **1994**, 1131.
(39) Chen, H. Y.; Archer, R. D. *Macromolecules* **1996**, *29*, 1957.
(40) Bekiari, V.; Pistolis, G.; Lianos, P. *Chem. Mater.* **1999**, *11*, 3189.
(41) Wang, L. H.; Wang, W.; Zhang, W. G.; Kang, E. T.; Huang, W. *Chem. Mater.* **2000**, *12*, 2212.
(42) Yan, B.; Qiao, X. F. *J. Phys. Chem. B.* **2007**, *111*, 12362.
(43) Xu, Q. H.; Li, L. S.; Li, B.; Xu, R. R. *Microporous Mesoporous Mater.* **2000**, *38*, 351.
(44) Fernandes, A.; Dexpert-Ghys, J.; Gleizes, A.; Galarneau, A.; Brunel, D. *Microporous Mesoporous Mater.* **2005**, *83*, 35.
(45) Zhang, M. S.; Yin, W.; Su, Q.; Zhang, H. J. *Mater. Lett.* **2002**, *57*, 940.
(46) Zhao, D. Y.; Huo, Q. S.; Feng, J. L.; Chmelka, B. F.; Stucky, G. D. *J. Am. Chem. Soc.* **1998**, *120*, 6024.
(47) Zhao, D. Y.; Feng, J. L.; Huo, Q. S.; Melosh, N.; Fredrickson, G. H.; Chmelka, B. F.; Stucky, G. D. *Science* **1998**, *279*, 548.
(48) Peng, C. Y.; Zhang, H, J.; Yu, J. B.; Meng, Q. G.; Fu, L. S.; Li, H. R.; Sun, L. N.; Guo, X. M. *J. Phys. Chem. B.* **2005**, *109*, 15278.
(49) Li, L. S.; Zhang, H, J.; Peng, C. Y.; Yu, J. B.; Meng, Q. G.; Fu, L. S.; Liu, F. Y.; Guo, X. M. *J. Phys. Chem. B.* **2006**, *110*, 7249.

Tb_4O_7) in concentrated nitric acid (HNO_3). Other starting reagents were used as received.

2.2. Synthetic Procedures. 2.2.1. Synthesis of Polymer Precursor (PMMA). Methyl methacrylate (1 mmol, 0.100 g) was dissolved in a small quantity of the solution THF (6 mL) with the initiator (BPO, benzoyl peroxide) to initiate the addition polymerization under argon atmosphere purging. The reaction temperature was maintained at 70 °C for about 6 h. The coating liquid was concentrated at room temperature to remove the solvent THF using a rotary vacuum evaporator, and the viscous liquid was obtained, identified as $[C_5H_8O_2]_n$ (see Figure 1A). It was dissolved in the solvent *N*,*N*-dimethyl formamide (DMF) for the coordinate reaction with rare earth ions later.

2.2.2. Synthesis of the Cross-Linking Precursor Containing Si−O Chemical Bonds (TTA-Si). The synthesis of TTA-Si was achieved according to the method in ref.[50]: 2-Thenoyltrifluoroacetone (TTA) (1 mmol, 0.222 g) was first dissolved in 20 mL of dehydrate THF, and NaH (2 mmol, 0.048 g) was added into the solution with stirring. Two hours later, 2.0 mmol (0.495 g) of 3-(triethoxysilyl)-propyl-isocyanate (TEPIC) was added dropwise into the refluxing solution. The mixture was heated at 65 °C in a covered flask for approximately 12 h in a nitrogen atmosphere. After isolation and purification, a yellow viscous liquid was obtained. TTA-Si ($C_{28}H_{47}O_{10}F_3N_2Si_2S$): IR: -CONH- 1630 cm^{-1}, -$(CH_2)_3$- 2970 cm^{-1}, Si−O 1090 cm^{-1}. ^{1}H NMR (DMSO): δ 8.06(2H, bs, NH), 8.02(H, s), 7.54(H, s), 7.27(H, bs), 3.85(12H, q, CH_2(OEt)), 3.27(4H, t), 1.85(4H, m,), 1.23(18H, t, CH_3(OEt)), 0.74(4H, t). ^{13}CNMR: δ5.1 (CH_2*Si*), δ7.35 (*O*=*C*CH_2*C*=*O*), δ18.4 (CH_3*CH_2O*), δ23.1 (*CH_2*CH_2*CH_2*), δ42.0 (*N*CH_2*CH_2*), δ58.1 (*CH_3*CH_2O*), δ120.5 (*CH* = CH*S*), δ124.7 (*CH*=CH*CH*=*C*), δ126.2 (*CH*CH=*CSC*=*O*), δ127.4 (*CH*=C*SC*=*O*), δ129.3 (*CF_3*), δ149.3 (C(*C*=*O*)$_2$), δ157.8 (*SC*C=*OC*), δ178.9 (*CF_3*C=*O*). Therefore, we could infer that the precursor TTA-Si has been synthesized successfully proved by the data.

2.2.3. Synthesis of TTA-Functionalized SBA-15 Material (TTA-SBA-15). TTA-functionalized SBA-15 mesoporous material was synthesized from acidic mixture with the following molar composition 0.0172 P123:0.96 TEOS:0.04 TTA-Si:6 HCl:208.33 H_2O. P123 (1.0 g) was dissolved in deionized water (7.5 g) and 2 M HCl solution (30 g) at 35 °C. A mixture of TTA-Si and TEOS was added into the above solution at 35 °C with stirring for 24 h and transferred into a Teflon bottle sealed in an autoclave, which was heated at 100 °C for 48 h. Then the solid product was filtrated, washed thoroughly with deionized water, and air-dried for 12 h at 60 °C. Removal of copolymer surfactant P123 was conducted by Soxhlet extraction with ethanol under reflux for 2 days to give the sample denoted as TTA-SBA-15.

2.2.4. Synthesis of SBA-15 Mesoporous Materials and Polymer Covalently Bonded with Ln^{3+} Complexes (denoted as Ln(TTA-SBA-15)$_3$PMMA. Ln = Eu, Tb). The precursors TTA-SBA-15 and PMMA were dissolved in DMF solvent, and an appropriate amount of $Ln(NO_3)_3$ ethanol solution was added into the solution while stirring (the molar ratio of Ln^{3+}: TTA-SBA-15: PMMA = 1:3:1). The mixture was stirred at room temperature for 12 h, followed by filtration and extensive washing with EtOH. The resulting material Ln(TTA-SBA-15)$_3$PMMA was dried overnight at 60 °C under vacuum environment. The predicted structure of Ln(TTA-SBA-15)$_3$PMMA was obtained as outlined in Figure 1B.

2.2.5. Synthesis of SBA-15 Mesoporous Material Covalently Bonded with the Binary Ln^{3+} Complexes (Denoted as Ln(TTA-SBA-15)$_3$, Ln = Eu, Tb). The synthesis procedure for Ln (TTA-SBA-15)$_3$ was similar to that of Ln(TTA-SBA-15)$_3$PMMA except that the precursors TTA-SBA-15 and PMMA were replaced by TTA-SBA-15.

2.3. Physical Measurement. FTIR spectra were meaured within the 4000−400 cm^{-1} region on an infrared spectrophotometer with the KBr pellet technique. ^{1}H NMR and ^{13}CNMR spectra were recorded in DMSO on a BRUKER AVANCE-500 spectrometer with tetramethylsilane (TMS) as inter reference. The ultraviolet absorption spectra were taken with an Agilent 8453 spectrophotometer. X-ray powder diffraction patterns were recorded on a Rigaku D/max-rB diffractometer equipped with a Cu anode in a 2θ range from 0.6° to 6°. Nitrogen adsorption/desorption isotherms were measured at the liquid nitrogen temperature, using a Nova 1000 analyzer. Surface areas were calculated by the Brunauer−Emmett−Teller (BET) method and pore size distributions were evaluated from the desorption branches of the nitrogen isotherms using the Barrett−Joyner−Halenda (BJH) model. The fluorescence excitation and emission spectra were obtained on a RF-5301 spectrophotometer. Luminescence lifetime measurements were carried out on an Edinburgh FLS920 phosphorimeter using a 450 w xenon lamp as excitation source. Scanning electronic microscope (SEM) was measured on Philips XL-30. Transmission electron microscope (TEM) experiments were conducted on a JEOL2011 microscope operated at 200 kV or on a JEM-4000EX microscope operated at 400 kV. Thermogravimetric analysis (TGA) was performed on a Netzsch STA 409 at a heating rate of 15 °C/min under nitrogen atmosphere.

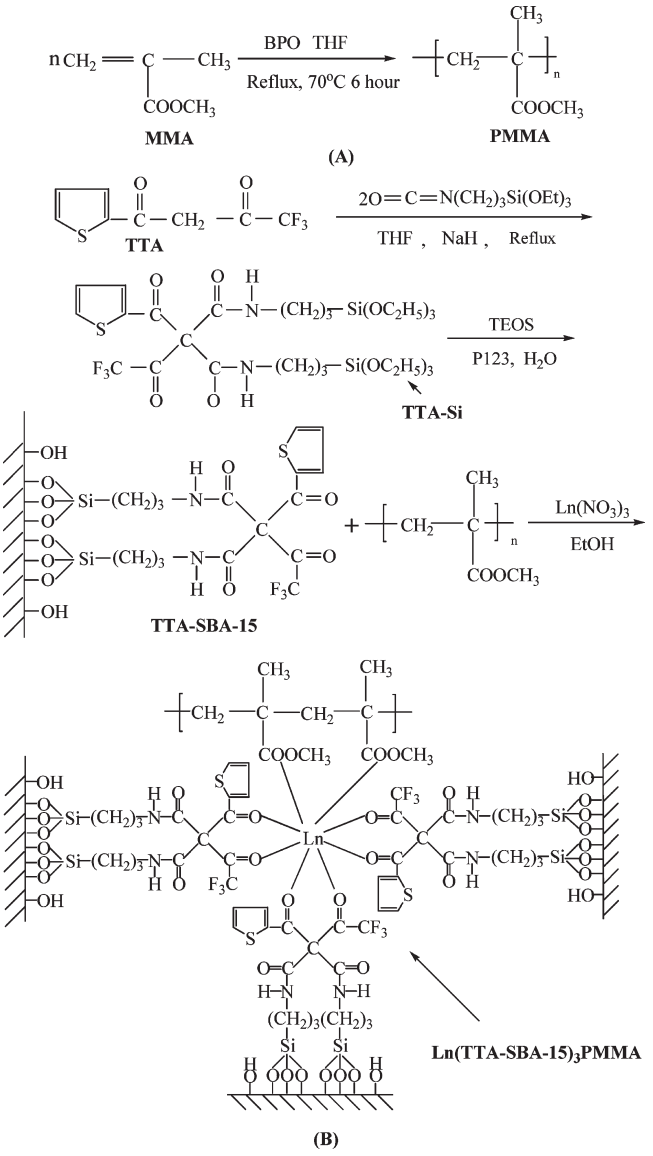

Figure 1. (A) Scheme of synthesis of polymer precursor PMMA. (B) Scheme of the synthesis process of the mesoporous polymeric hybrid materials Ln(TTA-SBA-15)$_3$PMMA.

(50) Qiao, X. F.; Yan, B. *Inorg. Chem.* **2009**, *48*, 4714.

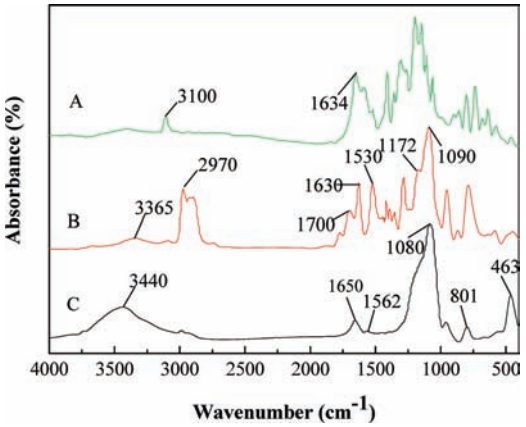

Figure 2. IR spectra of the free ligand TTA (A), the precursor TTA-Si (B), and the mesoporous hybrid material TTA-SBA-15 (C).

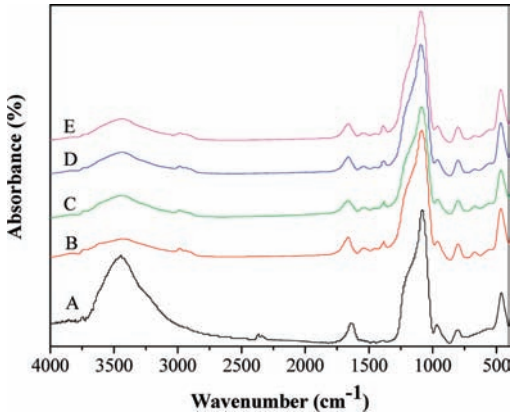

Figure 3. IR spectra of SBA-15 (A), Eu(TTA-SBA-15)$_3$ (B), Eu(TTA-SBA-15)$_3$PMMA (C), Tb(TTA-SBA-15)$_3$ (D), and Tb(TTA-SBA-15)$_3$PMMA (E).

3. Results and Discussion

3.1. FTIR Spectra. The IR spectra of the free β-diketone ligand (TTA), the precursor (TTA-Si), and TTA-functionalized hybrid mesoporous material are shown in Figure 2 (A, TTA; B, TTA-Si; C, TTA-SBA-15). In view of free ligand TTA (A), the vibration of $-CH_2-$ at 3100 cm^{-1} was replaced by a strong broadband located at 2970 cm^{-1}, which originated from the three methylene groups of 3-(triethoxysilyl)-propyl isocyanate (TEPIC). In addition, the spectra of TTA-Si is dominated by ν (C−Si, 1172 cm^{-1}) and ν (Si−O, 1090 cm^{-1}) absorption bands, characteristic of trialkoxylsilyl functions, which is the evidence of the emergence of TTA-Si. The band centered at 3365 cm^{-1} corresponds to the stretching vibration of grafted −NH− groups. Moreover, the bending vibration (δ_{NH}, 1530 cm^{-1}) further proves the formation of amide groups. New bands at 1700 and 1630 cm^{-1} in B were attributed to the absorptions of the C═O absorptions of TEPIC, proving that 3-(triethoxysilyl)-propyl isocyanate was successfully grafted onto the ligand TTA. The spectra of mesoporous hybrid material (C) indicated the formation of a Si−O−Si framework, which is evidenced by the broad bands located at 1080 cm^{-1} (ν_{as}, Si−O), 801 cm^{-1} (ν_s, Si−O), and 463 cm^{-1} (δ, Si−O−Si), which is attributed to the success of hydrolysis and copolycondensation[51] (ν represents stretching, δ represents plane bending, *s* represents symmetric, and *as* represents asymmetric vibrations). Furthermore, the bands at 1650 and 1562 cm^{-1} originating from −CONH− group of TTA-Si, can also be observed in panel C of Figure 2, which is consistent with the fact that the TTA group in the framework remains intact after both hydrolysis−condensation reaction and the surfactant extraction procedure.[52]

The IR spectra of SBA-15 (A), Eu(TTA-SBA-15)$_3$ (B), Eu(TTA-SBA-15)$_3$PMMA (C), Tb(TTA-SBA-15)$_3$ (D), and Tb(TTA-SBA-15)$_3$PMMA (E) are shown in Figure 3. In the SBA-15 host material (A), the evident bands appearing at 1080 cm^{-1} are due to asymmetric Si−O stretching vibration modes(ν_{as}, Si−O), and the band at 795 cm^{-1} can be attributed to the symmetric Si−O stretching vibration (ν_s, Si−O).The Si−O−Si bending vibration (δ, Si−O−Si) can also be observed at 472 cm^{-1}, and the band at 962 cm^{-1} is associated with silanol (Si−OH) stretching vibrations of surface groups.[53] In addition, the presence of hydroxyl can be clearly evidenced by the band at 3440 cm^{-1}. Compared with SBA-15, the hybrid mesoporous materials Ln(TTA-SBA-15)$_3$, Ln(TTA-SBA-15)$_3$PMMA (Ln = Eu, Tb) not only exhibit the similar infrared absorption bands as the silica framework but also the bands in the 1350−1560 cm^{-1} range, which just originate from the −CONH− group of TTA-Si, indicating that TTA-Si has been grafted onto the wall of SBA-15. The IR data of all these materials are listed in Table 1.

3.2. Ultraviolet Absorption Spectra. Figure 4 exhibits ultraviolet absorption spectra of TTA (A), TTA-Si (B), TTA-SBA-15 (C), and Eu(TTA-SBA-15)$_3$PMMA (D). From the spectra, it can be observed that an obvious blue shift of the major $\pi-\pi^*$ electronic transitions A→B (from 266 to 257 nm) occurred and a broadband at 333 nm appeared, which indicates that the electron distribution of the modified TTA-Si has changed compared to free ligand TTA because of the introduction of carbonyl group, and 3-(triethoxysilyl)-propyl isocyanate has been grafted to the ligand TTA successfully. In terms of B and C, the band shape has not changed basically, but an obvious red shift (257→260, 333→337 nm) is observed, suggesting that a more extensive $\pi-\pi^*$ conjugating system was formed owing to the grafting reaction, and the TTA groups were located on the surface of the mesoporous material SBA-15.[54] After the coordinate reactions, the absorption spectra of the hybrid material D (Eu(TTA-SBA-15)$_3$PMMA) are a little different from those of C (TTA-SBA-15). The bands at about 260 and 337 nm in C have shifted to 269 and 348 nm in D, respectively, which indicates the formation of a conjugated system between TTA-SBA-15, Eu^{3+}, and PMMA, different from the conjugated system between that in C. Because PMMA and TTA-SBA-15 coordinate with rare-earth ions Ln^{3+} simultaneously, a steadier conjugated system between them forms in the rare earth complex/polymer hybrids with the organic/inorganic networks synthesized through cohydrolysis, copolycondensation, and addition polymerization,

(51) Franville, A. C.; Mahiou, R.; Zambon, D.; Cousseins, J. C. *Solid State Sci.* **2001**, *3*, 211.
(52) Li, H. R.; Lin, J.; Fu, L. S.; Guo, J. F.; Meng, Q. G.; Liu, F. Y.; Zhang, H. J. *Microporous Mesoporous Mater.* **2002**, *55*, 103.
(53) Landau, M. V.; Parkey, S. P.; Herskowitz, M.; Regev, O.; Pevzner, S.; Sen, T.; Luz, Z. *Microporous Mesoporous Mater.* **1999**, *33*, 149.
(54) Wang, Q. M.; Yan, B. *J. Mater. Res.* **2005**, *20*, 592.

Table 1. Main Bands and Their Assignments of FTIR Spectra for SBA-15, Ln(TTA-SBA-15)$_3$, and Ln(TTA-SBA-15)$_3$PMMA (Ln = Eu, Tb)

materials	ν_{as}(Si−O)	ν_s(Si−O)	δ(Si−O−Si)	ν(Si−OH)	ν(OH)
SBA-15	1080	795	472	962	3440
Eu(TTA-SBA-15)$_3$	1080	798	471	960	3425
Eu(TTA-SBA-15)$_3$PMMA	1090	798	471	960	3430
Tb(TTA-SBA-15)$_3$	1090	798	467	960	3430
Tb(TTA-SBA-15)$_3$PMMA	1090	798	467	960	3430

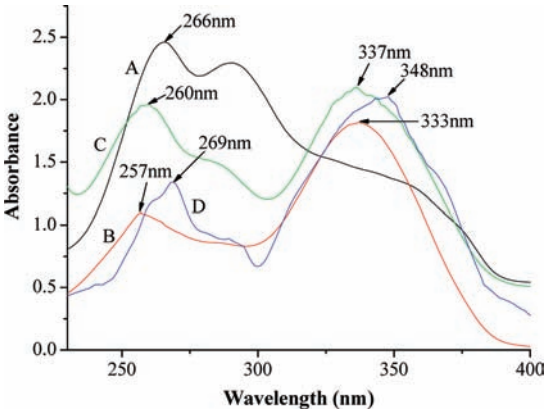

Figure 4. Ultraviolet absorption spectra of (A) TTA, (B) TTA-Si, (C) TTA-SBA-15, and (D) Eu(TTA-SBA-15)$_3$PMMA.

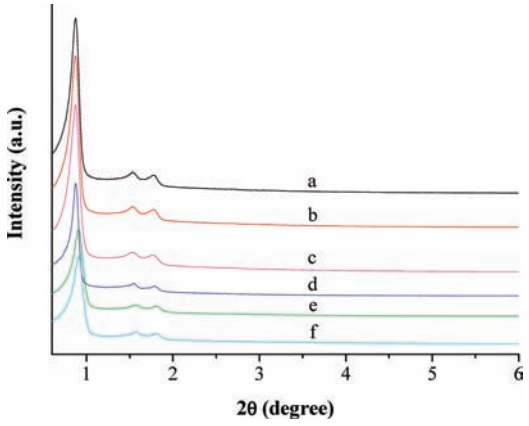

Figure 5. SAXRD patterns of SBA-15 (a), TTA-SBA-15 (b), Eu(TTA-SBA-15)$_3$ (c), Eu(TTA-SBA-15)$_3$PMMA (d), Tb(TTA-SBA-15)$_3$ (e), and Tb(TTA-SBA-15)$_3$PMMA (f).

which is different from the conjugated system merely with the simple inorganic network in C.[42]

3.3. X-ray Diffraction. The SAXRD patterns of pure SBA-15, TTA-SBA-15, Ln(TTA-SBA-15)$_3$, and Ln(TTA-SBA-15)$_3$PMMA (Ln=Eu^{3+}, Tb^{3+}) are shown in Figure 5. It can be seen that all samples exhibit three well-resolved diffraction bands in the 2θ range of 0.6−2°, which are indexed as the (100), (110), and (200) diffractions, characteristic of SBA-15-type two-dimensional hexagonal (*P6mm*). Compared with the SAXRD pattern of parent TTA-SBA-15 material, the d_{100} spacing values of the Ln(TTA-SBA-15)$_3$ and Ln(TTA-SBA-15)$_3$PMMA are nearly unchanged (see Table 2), indicating that the framework hexagonal ordering has been preserved well upon the introduction of Ln^{3+}. In addition, it can be observed that the lanthanide complex functionalized materials show a slight decrease in diffraction intensity in comparison with the parent TTA-SBA-15 material, which is probably due to the presence of guest moieties onto the mesoporous framework of SBA-15, resulting in the decrease of crystallinity but not the collapse in the pore structure of mesoporous materials.[55] It was reported that the introduction of guest into the pores leads to an increased phase cancellation between the guest moiety from the wall and the pore regions and accordingly to reduced scattering intensities for the Bragg reflections[50]

3.4. Nitrogen Sorption Measurement. To further investigate the channel structure of these materials, the characterization of the nitrogen adsorption−desorption was also carried out. The corresponding isotherms are displayed in Figure 6. They all exhibit typical type IV isotherms with distinct H1-type hysteresis loops at high relative pressures according to the IUPAC classification,[50,56−59] characteristic of mesoporous materials with highly uniform size distributions. From Figure 6, they all display distinct capillary condensation steps in the P/P_0 region from 0.45 to 0.80, indicating that the materials possess a well-defined array of regular mesopores. The inflection position shifted slightly toward lower relative pressures, and the volume of nitrogen adsorbed decreased with functionalization, which was indicative of a reduction in pore size.[60,61] Table 2 summarized the structural data of all these mesoporous materials, such as the BET surface area (S_{BET}), total pore volume and BJH average pore diameter, etc. It is known from Table 2, the pure SBA-15 possessed very high S_{BET} of 746 m^2/g, a large pore volume of 0.97 cm^3/g, and a BJH pore diameter of 5.64 nm, indicative of its potential application as a host in luminescent materials. After the functionalization with TTA, the TTA-SBA-15 exhibits a smaller surface area and a slightly smaller pore size and pore volume, which might be attributed to the presence of organic ligand TTA on the surface and co-surfactant effect of TTA-Si, which interacts with surfactant and reduces the diameter of the micelles.[62,63] Furthermore, it can be observed that the values of the S_{BET}, D, and v of materials decrease after introducing Ln^{3+} ions, which further confirmed incorporation of the Ln^{3+} complexes in the channels of SBA-15.

(55) Sun, L. N.; Yu, J. B.; Zhang, H. J.; Meng, Q. G.; Ma, E.; Peng, C. Y.; Yang, K. Y. *Microporous Mesoporous Mater.* **2007**, *98*, 156.
(56) Everett, D. H. *Pure Appl. Chem.* **1972**, *31*, 577.
(57) Sing, K. S. W.; Everett, D. H.; Haul, R. A. W.; Moscou, L.; Pierotti, R. A.; Rouquerol, J.; Siemieniewska, T. *Pure. Appl. Chem.* **1985**, *57*, 603.
(58) Kruk, M.; Jaroniec, M. *Chem. Mater.* **2001**, *13*, 3169.
(59) Zhang, W. H.; Lu, X. B.; Xiu, J. H.; Hua, Z. L.; Zhang, L. X.; Robertson, M.; Shi, J. L.; Yan, D. S.; Holmes, J. D. *Adv. Funct. Mater.* **2004**, *14*, 544.
(60) Jarupatrakorn, J.; Tilley, T. D. *J. Am. Chem. Soc.* **2002**, *124*, 8380.
(61) Xue, X. M.; Li, F. T. *Microporous Mesoporous Mater.* **2008**, *116*, 116.
(62) Peng, C. Y.; Zhang, H. J.; Meng, Q. G.; Li, H. R.; Yu, J. B.; Guo, F. J.; Sun, L. N. *Inorg. Chem. Commun.* **2005**, *8*, 440.
(63) Gao, B. J.; Yang, Y. F.; Cheng, Y.; Shi, D. J. *Spectrosc. Spectra Anal.* **2002**, *22*, 371.

Table 2. Structural Parameters of SBA-15, TTA-SBA-15, Ln(TTA-SBA-15)$_3$, and Ln(TTA-SBA-15)$_3$PMMA (Ln = Eu, Tb)[a]

sample	d_{100} (nm)	a_0 (nm)	S_{BET} (m^2/g)	V (cm^3/g)	D (nm)	t (nm)
SBA-15[35]	10.68	12.33	746	0.97	5.64	6.69
TTA-SBA-15	10.21	11.79	675	0.82	5.37	6.42
Eu(TTA-SBA-15)$_3$	9.66	11.15	589	0.76	5.19	5.96
Eu(TTA-SBA-15)$_3$PMMA	9.54	11.02	563	0.73	5.18	5.84
Tb(TTA-SBA-15)$_3$	9.57	11.05	462	0.58	5.05	6.00
Tb(TTA-SBA-15)$_3$PMMA	9.39	10.84	416	0.52	5.04	5.80

[a] d_{100} is the d(100) spacing, a_0 the cell parameter ($a_0 = 2\,d_{100}/\sqrt{3}$), S_{BET} the BET surface area, V the total pore volume, D_{BJH} the average pore diameter, and t the wall thickness, calculated by $a_0 - D$.

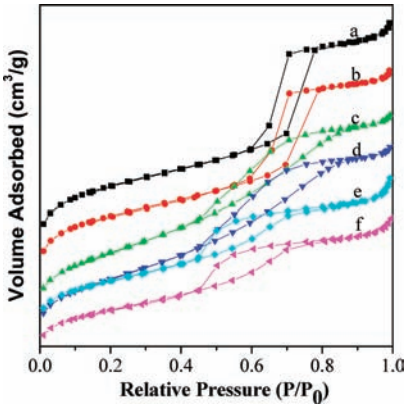

Figure 6. N_2 adsorption-desoption isotherms of SBA-15 (a), TTA-SBA-15 (b), Eu(TTA-SBA-15)$_3$ (c), Eu(TTA-SBA-15)$_3$PMMA (d), Tb-(TTA-SBA-15)$_3$ (e), and Tb(TTA-SBA-15)$_3$PMMA (f).

3.5. Transmission Electron Microscopy. The hexagonal mesostructures of Eu(TTA-SBA-15)$_3$PMMA are further confirmed by a TEM micrograph (see Figure 7). As shown in the figure, the lanthanide-complex-functionalized mesoporous material Eu(TTA-SBA-15)$_3$PMMA presents a regular hexagonal array of uniform channels characteristic of mesoporous SBA-15 material, which indicates that the mesostructure of Eu(TTA-SBA-15)$_3$PMMA can be substantially conserved after the complexation process. The distances between the centers of the mesopore is estimated to be around 11 nm, which is in good agreement with the value determined from the corresponding XRD data (see Table 2).

3.6. Scanning Electron Micrographs. Figure 8 present the microstructures of the molecular-based mesoporous hybrid polymeric materials Eu(TTA-SBA-15)$_3$PMMA (A) and Tb(TTA-SBA-15)$_3$PMMA (B). The scanning electron micrographs demonstrate that the homogeneous, molecular-based materials were obtained because of strong covalent bonds between the organic β-diketone ligand and the inorganic matrixes, and the coordinate bonds between organic ligand β-diketone or polymer ligand and rare earth ions, which belong to a complicated huge molecular system in nature. Compared with the hybrid materials with doped lanthanide complexes generally experiencing the phase separation phenomena, in this paper, the inorganic and organic phases can exhibit their distinct properties together in the hybrid materials we obtained containing covalent bonds. Furthermore, comparing the two SEM pictures, there exist distinct differences between the two kinds of mesoporous hybrid polymeric materials, which may be assigned to the difference of the central metal ions.

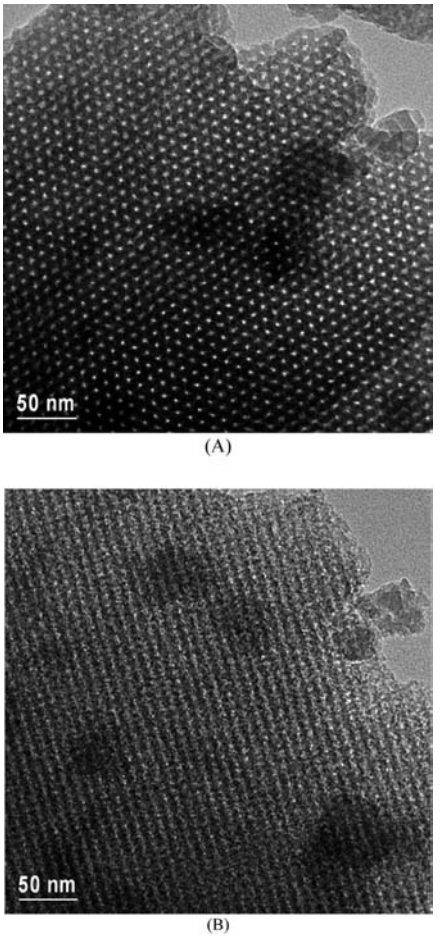

Figure 7. HRTEM images of Eu(TTA-SBA-15)$_3$PMMA recorded along the [100] (A) and [110] (B) zone axes.

3.7. Thermogravimetric Analysis (TGA). Figure 9 shows the TGA traces of the mesoporous hybrid materials Tb-(TTA-SBA-15)$_3$ (A) and Tb(TTA-SBA-15)$_3$PMMA (B). From the TGA curves we can see that, both the samples show the similar change trends in weight loss, and three main degradation steps can be observed. The first step of weight loss (about 4.8% for Tb(TTA-SBA-15)$_3$ and 7.0% for Tb(TTA-SBA-15)$_3$PMMA) from 30 to 160 °C could be attributed to the desorption of physically absorbed water and residual solvent, without any decomposition of the chemical bonds, which is an endothermic process observed from the DSC curves (not given). The second weight loss (about 10.8% for Tb(TTA-SBA-15)$_3$ and 10.6% for Tb-(TTA-SBA-15)$_3$PMMA) between 160 and 450 °C in heat flow around 381 °C was assigned to the loss of the thermal degradation of the mesoporous material framework.

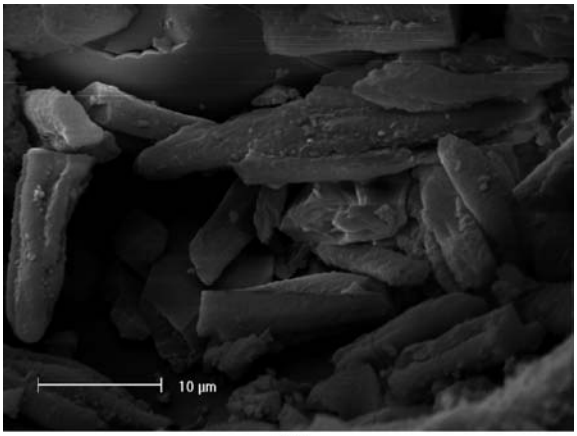

(A)

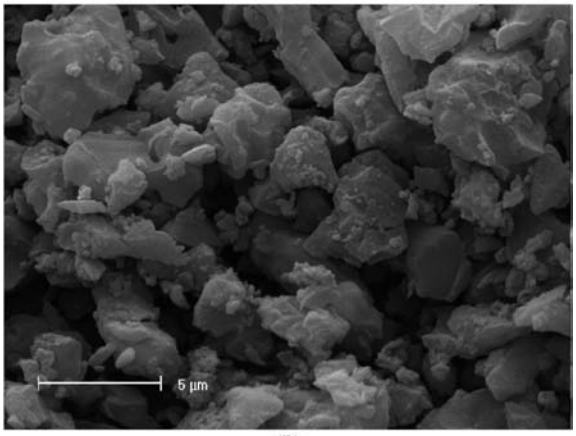

(B)

Figure 8. SEM images of the mesoporous polymeric hybrid materials Eu(TTA-SBA-15)$_3$PMMA (A) and Tb(TTA-SBA-15)$_3$PMMA (B).

Finally, the weight loss beyond 450 °C is due to the decomposition of organic ingredients. In addition, compared with the weight loss peak (approximately 10% at about 522 °C) of the binary mesoporous hybrid material Tb(TTA-SBA-15)$_3$, the decomposition point (about 552 °C) of the ternary mesoporous polymeric hybrid material Tb(TTA-SBA-15)$_3$PMMA is higher than that of Tb(TTA-SBA-15)$_3$, indicating that the thermal stability of mesoporous hybrid material after introducing the second ligand PMMA has been improved.

3.8. Photoluminescence Properties. The luminescence behavior of lanthanide hybrid mesoporous materials have been investigated at room temperature. The intramolecular energy transfer from the sensitizer to the central ions in the two kinds of hybrid mesoporous materials are investigated by energy difference between the triplet state energy of organic ligands and the accepting energy level of the central Ln^{3+} (Eu^{3+}, Tb^{3+}) ion. According to the energy match principle and intramolecular energy transfer mechanism,[64−67] the organic ligands absorb the energy in the ultraviolet region and then transfer the energy to the

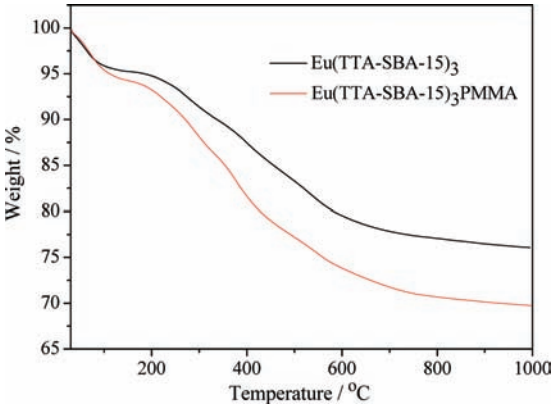

Figure 9. TGA curves of Tb(TTA-SBA-15)$_3$ (A) and Tb(TTA-SBA-15)$_3$PMMA (B).

accepting energy level of lanthanides ions with an intramolecular energy transfer process. The intramolecular energy transfer efficiency depends chiefly on the energy difference (ΔE ($T_r - Ln^{3+}$)) between the lowest triplet energy level of ligands and the accepting energy level of Ln^{3+}. On the basis of the above facts, there should exists an optimal energy difference between the triplet position of TTA and the accepting energy level of Ln^{3+} (Eu^{3+}, Tb^{3+}), the larger or the smaller ΔE ($T_r - Ln^{3+}$) value will decrease the luminescence properties of rare earth. Thus, the energy difference between the lowest triple state energy of the ligand TTA (20400 cm^{-1}) and the accepting energy level of Eu^{3+} ($^5D_0$, 17265 cm^{-1}), Tb^{3+} ($^5D_4$, 20500 cm^{-1}) were calculated,[68−71] and it can be predicted that the triplet state energy of the ligand TTA is more suitable for the luminescence of Eu^{3+} ion than for Tb^{3+} ion in the resulting materials. So, the mesoporous hybrid materials containing Eu^{3+} exhibit the better luminescence properties. The above estimation has been proven in the following photoluminescence spectra.

The excitation and emission spectra of the resulting hybrid mesoporous materials containing Eu^{3+} are shown in Figure 10 (A for Eu(TTA-SBA-15)$_3$, and B for Eu(TTA-SBA-15)$_3$PMMA). The excitation spectra were obtained by monitoring the emission of Eu^{3+} ions at 613 nm and are dominated by a series of broad bands centered at about 343−354 nm in the ultraviolet region which are the characteristic absorption of lanthanide complexes arising from the efficient transition based on the conjugated C=O double bonds of 2-thenoyltrifluoroacetone. As a result, the strong red luminescence was observed in their emission spectra, which indicates that the effective energy transfer took place and conjugated systems formed between the ligands and the chelated rare-earth ions in hybrids A and B. The emission bands of the mesoporous materials were assigned to the $^5D_0 \rightarrow 7F_J$ ($J = 0-4$) transitions at 576, 582, 613, 648, and 695 nm under excitation at wavelengths of 343, 354. The hybrid mesoporous materials show relatively strong emissions due to the chemically covalently bonded molecular Si−O network structure between the complexes and the mesoporous silica. As seen from Figure 10b, among the transitions of the materials containing Eu^{3+}, the $^5D_0 \rightarrow {}^7F_2$

(64) Dexter, D. L. *J. Chem. Phys.* **1953**, *21*, 836.
(65) Brown, T. D.; Shepherd, T. M. *J. Chem. Soc., Dalton Trans.* **1973**, 336.
(66) Yan, B.; Zhang, H. J.; Wang, S. B.; Ni, J. Z. *J. Photochem. Photobiol., A: Chem* **1998**, *116*, 209.
(67) Crosby, G. A.; Whan, R. E.; Alire, R. M. *J. Chem. Phys.* **1961**, *34*, 745.
(68) Yan, B.; Xu. B. *Spectrochim. Acta, Part A.* **2005**, *62*, 269.
(69) Wang, Q. M.; Yan, B. *J. Photochem. Photobiol, A: Chem.* **2006**, *178*, 70.
(70) Sato, S.; Wada, M. *Bull. Chem. Soc. Jpn.* **1970**, *43*, 1955.
(71) Wu, S. L.; Wu, Y. L.; Yang, Y. S. *J. Alloys Compd.* **1992**, *180*, 399.

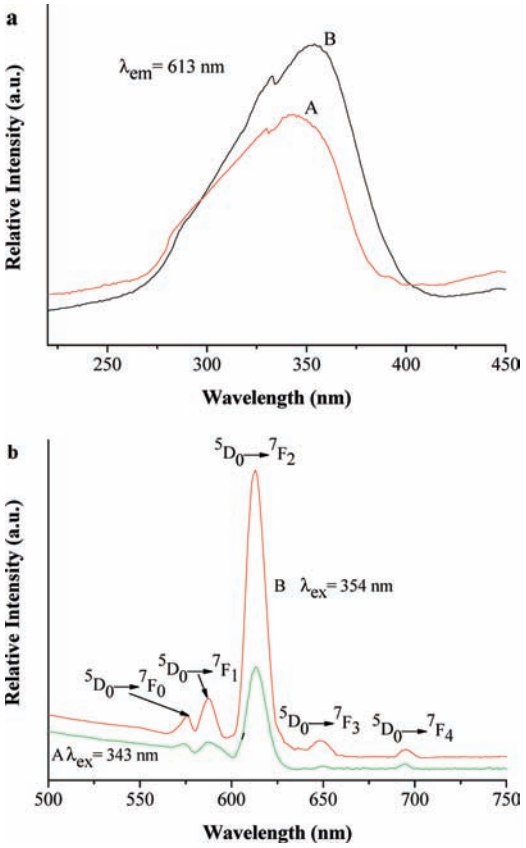

Figure 10. Fluorescent excitation (a) and emission (b) spectra of the mesoporous hybrid materials: (A) Eu(TTA-SBA-15)$_3$ and (B) Eu(TTA-SBA-15)$_3$PMMA.

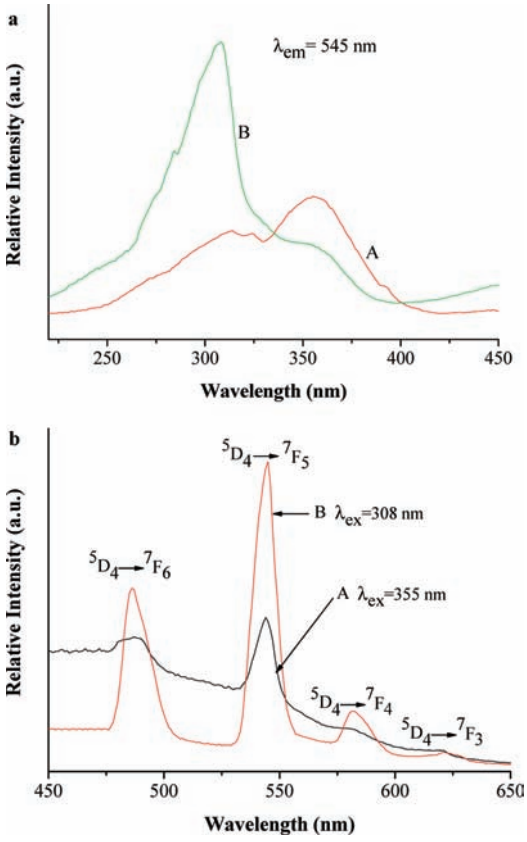

Figure 11. Fluorescent excitation (a) and emission (b) spectra of the mesoporous hybrid materials: (A) Tb(TTA-SBA-15)$_3$ and (B) Tb(TTA-SBA-15)$_3$PMMA.

at about 613 nm show the strongest emission. It is well-known that the $^5D_0 \rightarrow {}^7F_2$ transition is a typical electric dipole transition and strongly varies ;with the local symmetry of Eu^{3+}, while the $^5D_0 \rightarrow {}^7F_1$ transition corresponds to a parity-allowed magnetic dipole transition, which is independent of the host material. Therefore, the emission spectra indicate that the Eu^{3+} site is situated in an environment without inversion symmetry. Therefore, it is indicated that the effective energy transfer took place between the precursors and the chelated rare earth ions.[72−74]

Furthermore, we compared the luminescent relative intensities and lifetimes of the two mesoporous hybrid materials Eu(TTA-SBA-15)$_3$ and Eu(TTA-SBA-15)$_3$PMMA, and the detailed data have been listed in Table 2. Compared to binary complex Eu(TTA-SBA-15)$_3$, the relative emission intensities and luminescent lifetimes of ternary complexes Eu(TTA-SBA-15)$_3$PMMA exhibit obvious enhancements. We predicted that two reasons may contribute to the improved luminescence. One is that the oxygen atoms in ester groups located in the polymer chains of PMMA coordinate to Eu^{3+} ions, which replace the coordinated water molecules existing in complexes of aromatic carboxylic acid ligands, and the energy loss and clustering of the emitting centers caused by the vibration of the hydroxyl groups of coordinated water molecules could be avoided. The additional reason is that the more effective energy transfer took place from PMMA to the chelated Eu^{3+} ions; through this efficient method, leaching of the photoactive molecules can be avoided, a higher concentration of metal ions can be obtained, and clustering of the emitting centers can be prevented because the hybrids belong to the molecular level. Besides, we simply compare the luminescent property of the mesoporous hybrids with a PMMA polymer chain with that of ternary mesoporous hybrids with a second photoactive molecule such as 1,10-phenanthroline. [35] Unfortunately, it is found that the former is not better than the latter, which suggests that the structural influence of the PMMA polymer chain is not so effective as the direct sensitization of 1,10-phenanthroline on the luminescence of the whole hybrid system.[35]

Figure 11 presents the excitation and emission spectra of Tb(TTA-SBA-15)$_3$ and Tb(TTA-SBA-15)$_3$PMMA mesoporous materials. The excitation spectra of resulting mesoporous materials are similar, which were obtained by monitoring the corresponding emission wavelength of the Tb^{3+} ion at 545 nm. As shown in Figure 11a, a broadband ranging from 220 to 450 nm can be seen, which can be ascribed to the $\pi \rightarrow \pi^*$ electron transition of the ligands.[75] The emission bands of the mesoporous hybrid materials obtained from the $^5D_4 \rightarrow {}^7F_J$ (J = 3−6) transitions at 488,

(72) Latva, M.; Takal, H.; Mukkala, V.; Matachescuc, C. *J. Lumin.* **1997**, *75*, 149.
(73) Miranda, J. P.; Zukerman-Schpector, J.; Isolani, P. C.; Vicentini, G.; Zinner, L. B. *J. Alloys Compd.* **2002**, *344*, 141.
(74) Guo, X. M.; Fu, L. S.; Zhang, H. J.; Carlos, L. D.; Peng, C. Y.; Guo, J. F.; Yu, J. B.; Deng, R. P.; Sun, L. N. *New J. Chem.* **2005**, *29*, 1351.
(75) Li, H. H.; Inoue, S.; Machida, K.; Adachi, G. *Chem. Mater.* **1999**, *11*, 3171.

Table 3. Photoluminescent Data of Ln(TTA-SBA-15)$_3$ and Ln(TTA-SBA-15)$_3$PMMA (Ln = Eu, Tb)

hybrids	λ_{em} (nm)	I (a.u.)	τ^c (ms)	$1/\tau$ (s^{-1})	A_r	A_{nr}	η (%)
Eu(TTA-SBA-15)$_3$	574	100.60					
	587	103.30					
	613	246.89	0.32	3125	288	2837	9.2
	650	57.15					
	695	61.54					
Eu(TTA-SBA-15)$_3$PMMA	576	153.53					
	587	186.40					
	613	622.95	0.48	2083	332	1751	16.0
	648	106.45					
	695	89.07					
Tb(TTA-SBA-15)$_3$	487	200.49	0.13	7692			
	544	229.21					
Tb(TTA-SBA-15)$_3$PMMA	486	272.77					
	545	460.90	0.28	3571			
	582	90.00					
	621	29.15					

544, 582, and 622 nm under excitation at wavelengths of 308 and 355 nm. As for the binary complex Tb(TTA-SBA-15)$_3$, we could observe only two bands at 486 and 541 nm originating from $^5D_4 \rightarrow {}^7F_6$ and $^5D_4 \rightarrow {}^7F_5$, respectively, while the bands originating from $^5D_4 \rightarrow {}^7F_4$ and $^5D_4 \rightarrow {}^7F_3$ transitions are so weak that they cannot be seen clearly from the emission spectra of the samples. This suggests that an inefficient energy transfer process occurred between TTA-Si and terbium ions. After the introduction of the organic ligand PMMA, the emission intensities of ternary complex Tb(TTA-SBA-15)$_3$PMMA show obvious enhancement, which indicates that the presence of both β-diketone ligand TTA and the second ligand PMMA could sensitize luminescent properties of Tb^{3+} ion.

3.9. Luminescent Decay Times (τ) and Emission Quantum Efficiency (η). The typical decay curves of the Eu^{3+} and Tb^{3+} hybrid mesoporous materials were measured, and they can be described as a single exponential in the orm $\ln[S(t)/S_0] = -k_1 t = -t/\tau$, indicating that all Ln^{3+} ions occupy the same average coordination environment. The resulting lifetimes of the Eu^{3+} and Tb^{3+} hybrids are given in Table. 3. It was found that the rare-earth/inorganic/organic ternary polymeric hybrids Ln(TTA-SBA-15)$_3$PMMA present longer luminescent lifetimes than the corresponding rare-earth/inorganic binary hybrids Ln(TTA-SBA-15)$_3$, which suggested that the introduction of an organic polymeric chain can enhance the luminescence stability of the overall hybrid system.

Furthermore, we selectively determined the emission quantum efficiencies (η) of the $^5D_0$ europium ion excited state for Eu^{3+} hybrids on the basis of the emission. Assuming that only non-radiative and radiative processes are essentially involved in the depopulation of the $^5D_0$ state, η can be defined as follows:[76]

$$\eta = \frac{A_r}{A_r + A_{nr}} \quad (1)$$

A_r can also be obtained by summing over the radiative rates A_{0J} for each of the $^5D_0 \rightarrow {}^7F_J$ ($J = 0-4$) transitions of Eu^{3+}.

$$A_r = \sum A_{0J} = A_{00} + A_{01} + A_{02} + A_{03} + A_{04} \quad (2)$$

The branching ratio for the $^5D_0 \rightarrow {}^7F_{5,6}$ transitions can be neglected as they are not detected experimentally, and whose influence can be ignored in the depopulation of the $^5D_0$ excited state. Since $^5D_0 \rightarrow {}^7F_1$ belongs to the isolated magnetic dipole transition, it is practically independent of the chemical environments around the Eu^{3+} ion, and thus can be considered as an internal reference for the whole spectrum; the experimental coefficients of spontaneous emission, A_{0J} can be calculated according to the equation[77-79]

$$A_{0J} = A_{01}(I_{0J}/I_{01})(\nu_{01}/\nu_{0J} \quad (3)$$

Here, A_{0J} are the experimental coefficients of spontaneous emission. A_{01} is the Einstein coefficient of spontaneous emission between the $^5D_0$ and $^7F_1$ energy levels. In vacuum, A_{01} has a value of 14.65 s^{-1}, when an average index of refraction n equal to 1.506 was considered, the value of A_{01} can be determined to be 50 s^{-1} approximately ($A_{01} = n^3 A_{01(vac)}$).[80] I_{01} and I_{0J} are the integrated intensities of the $^5D_0 \rightarrow {}^7F_1$ and $^5D_0 \rightarrow {}^7F_J$ transitions ($J = 0-4$) with ν_{01} and ν_{0J} ($\nu_{0J} = 1/\lambda_J$) energy centers, respectively. ν_{0J} refers to the energy barrier and can be determined from the emission bands of Eu^{3+}'s $^5D_0 \rightarrow {}^7F_J$ emission transitions. The emission intensity, I, taken as integrated intensity S of the $^5D_0 \rightarrow {}^7F_{0-4}$ emission curves, can be defined as below:

$$I_{i-j} = \hbar\omega_{i-j} A_{i-j} N_i \approx S_{i-j} \quad (4)$$

Here i and j are the initial ($^5D_0$) and final levels ($^7F_{0-4}$), respectively, ω_{i-j} is the transition energy, A_{i-j} is the

(76) Soares-Santos, P. C. R.; Nogueira, H. I. S.; Félix, V.; Drew, M. G. B.; Sá Ferreira, R. A.; Carlos, L. D.; Trindade, T. *Chem. Mater.* **2003**, *15*, 100.

(77) Teotonio, E. S.; Espínola, J. G. P.; Brito, H. F.; Malta, O. L.; Oliveria, S. F.; de Foria, D. L. A.; Izumi, C. M. S. *Polyhedron*. **2002**, *21*, 1837.

(78) Carlos, L. D.; Messaddeq, Y.; Brito, H. F.; Sá Ferreira, R. A.; de Zea Bermudez, V.; Ribeiro, S. J. L. *Adv. Mater.* **2000**, *12*, 594.

(79) Hazenkamp, M. F.; Blasse, G. *Chem. Mater.* **1990**, *2*, 105.

(80) Werts, M. H. V.; Jukes, R. T. F.; Verhoeven, J. W. *Phys. Chem. Chem. Phys.* **2002**, *4*, 1542.

Einstein coefficient of spontaneous emission, and N_i is the population of the $^5D_0$ emitting level. On the basis of refs 81−83, the value of $A_{01} \approx 50\ s^{-1}$ and the lifetime (τ), radiative (A_r), and non-radiative (A_{nr}) transition rates are related through the following equation:

$$\tau = (A_r + A_{nr})^{-1} \quad (5)$$

On the basis of the above discussion, it can be seen the value η mainly depends on the values of two factors: one is lifetimes and the other is I_{02}/I_{01}. If the lifetimes and red/orange ratio are large, the quantum efficiency must be high. As can be clearly seen from Table 3, the quantum efficiency of the ternary mesoporous polymeric hybrid kinds Ln(TTA-SBA-15)$_3$PMMA is higher than the binary mesoporous hybrid Ln(TTA-SBA-15)$_3$, which indicates that the addition of organic polymeric chain into the hybrids not only enhances the materials' luminescent intensities, but also extends the materials' luminescent lifetimes and thus improve the hybrid materials' quantum efficiencies.

4. Conclusion

In summary, ternary rare earth luminescent mesoporous hybrid materials Ln(TTA-SBA-15)$_3$PMMA (Ln = Eu, Tb) were successfully prepared by linking ternary lanthanide (Eu^{3+}, Tb^{3+}) complexes to the ordered mesoporous SBA-15 through the functionalized TTA-Si ligand, which provides a representative method for assembling mesoporous luminescent rare earth molecular-based polymeric hybrid materials with chemical bonds, containing the long organic carbon chains and ordered organic network (Si−O−Si) through the sol−gel process. All the resulting materials preserve their mesoscopically ordered structures and show highly uniform pore size distributions. Further investigation on the luminescence properties show that the mesoporous material covalently bonded Eu^{3+} complex exhibits the stronger characteristic emission of Eu^{3+} and longer lifetime than the Tb^{3+} complex because the triplet state energy of organic ligand TTA matches with the emissive energy level of Eu^{3+} very well. In addition, the ternary polymeric hybrid materials exhibit stronger luminescent intensities, longer lifetimes, and higher quantum efficiencies than binary ones for the introduction of organic ligand PMMA. The excellent luminescent properties of these materials, together with the highly ordered hexagonal channel structures and uniform tunable pore sizes of the organic group functionalized SBA-15 mesoporous materials will expand their applications in optical or electronic areas.

Acknowledgment. This work was supported by the National Natural Science Foundation of China (20671072) and Program for New Century Excellent Talents in University (NCET-08-0398).

(81) Boyer, J. C.; Vetrone, F.; Capobianco, J. A.; Speghini, A.; Bettinelli, M. *J. Phys. Chem. B.* **2004**, *108*, 20137.
(82) Frey, S. T.; Gong, M. L.; Horrocks, W. D., Jr. *Inorg. Chem.* **1994**, *33*, 3229.
(83) Malta, O. L.; Batista, H. J.; Carlos, L. D. *Chem. Phys.* **2002**, *282*, 21.